applied sciences

MDPI

Article

Simulation of Accelerated Subcritical Flow Profiles in an Open Channel with Emergent Rigid Vegetation

Antonino D'Ippolito [1,*], Francesco Calomino [1], Nadia Penna [1], Subhasish Dey [2] and Roberto Gaudio [1]

[1] Dipartimento di Ingegneria Civile, Università della Calabria, 87036 Rende, CS, Italy; francesco.calomino@unical.it (F.C.); nadia.penna@unical.it (N.P.); gaudio@unical.it (R.G.)
[2] Department of Civil Engineering, Indian Institute of Technology Kharagpur, Kharagpur 721302, West Bengal, India; sdey@iitkgp.ac.in
* Correspondence: antonino.dippolito@unical.it; Tel.: +39-984-496550

Abstract: Even though both fluid mechanics and numerical studies have considerably progressed in the past decades, experimental knowledge remains an important tool for studying the resistance to flow in fluid media where a complex environment dominates the flow pattern. After a comprehensive review of the recent literature on the drag coefficient in open channels with emergent rigid vegetation, this paper presents the results related to 29 experimental accelerated subcritical flow profiles (i.e., M2 type) that were observed in flume experiments with emergent stems in a square arrangement at the University of Calabria (Italy). First of all, we used some of the literature formulas for the drag coefficient, concluding that they were unsatisfactory, probably because of their derivation for uniform or quasi-uniform flow conditions. Then, we tested a recently proposed approach, but when we plotted the drag coefficient versus the stem Reynolds number, the calculated drag coefficients showed an inconclusive behavior to interpret. Thus, we proposed a new approach that considers the calibration of the Manning coefficient for the simulation of the free surface profile, and then the evaluation of the drag coefficients based on the fundamental fluid mechanics equations. With the help of classical dimensional analysis, a regression equation was found to estimate the drag coefficients by means of non-dimensional parameters, which include vegetation density, stem Reynolds number and flow Reynolds number computed using the flow depth as characteristic length. This equation was used to simulate all the 26 observed profiles and, also, 4 experimental literature profiles, and the results were good. The regression equation could be used to estimate the drag coefficient for the M2 profiles in channels with squared stem arrangements, within the range of vegetation densities, flow Reynolds numbers and stem Reynolds numbers of the present study. However, in the case of the three profiles observed by the authors for staggered arrangement, the regression equation gives significantly underestimated flow depths.

Keywords: river hydraulics; vegetation; flow resistance; drag coefficient; cylinder arrays

Citation: D'Ippolito, A.; Calomino, F.; Penna, N.; Dey, S.; Gaudio, R. Simulation of Accelerated Subcritical Flow Profiles in an Open Channel with Emergent Rigid Vegetation. *Appl. Sci.* **2022**, *12*, 6960. https://doi.org/10.3390/app12146960

Academic Editor: Francesca Scargiali

Received: 21 May 2022
Accepted: 7 July 2022
Published: 9 July 2022

1. Introduction

Vegetation has an important hydrological role at the basin scale because it reduces erosion and floods and increases infiltration [1–5]. On the other hand, vegetation along watercourses plays an important role in the river ecosystem, enhancing the landscape.

In relation to the river ecosystem, aquatic plants can improve water quality by producing oxygen, consume excess nutrients, decrease the suspended solids, provide a habitat for aquatic animals by creating low-flow areas and prevent fertilizers and pollutants from reaching the watercourses [6–9]. Projects for the renaturalization and rehabilitation of watercourses are currently underway worldwide [10–14].

From the hydrodynamic viewpoint, vegetation increases the flow resistance, changes the backwater profiles, modifies the sediment erosion and deposition [15] and influences

the river morphology [16]. These phenomena have a mutual interaction whose analysis becomes very complex owing to the various physical mechanisms involved and the biomechanical properties characterizing different types of vegetation [17,18].

Resistance due to vegetation varies in the main channel and the flood plains as a result of the vegetation flexibility, submergence, foliage and side-branching, type, height, density and spatial distribution of plants [19–21]. The effects that vegetation can exert on stream flow processes are further complicated by the temporal and spatial variations of flow stage, uniformity and steadiness [22].

As for river hydraulics, vegetation may occupy part of the river cross section [23–25], increasing the roughness and reducing the flow velocity: these result in increased flow levels and a reduced water conveyance. Moreover, while, on the one hand the lower average flow velocity reduces the erosion of the riverbed and banks [26], on the other hand it causes an increase of the sediment deposition, making the flow cross section smaller and, consequently, raising the flooding risk. At the scale of the hydrographic network, the general velocity reduction influences the travel time of water particles, making easier the peak flow to control [27]. With reference to the hydraulic aspects, the focus of researchers, in addition to the flow resistance, is on the analysis of turbulence characteristics [28–32] and solid transport [15,18,33–35].

Commonly, in the literature, vegetation is considered to be rigid or flexible and, according to the flow depth, as emergent or submerged. In laboratory experiments, rigid vegetation is usually represented by rigid cylinders of various materials and sizes [36].

The aim of this study is to recognize how the drag coefficient varies in the case of emergent rigid vegetation in a gradually varied flow (GVF) profile, which apparently differs from the cases of uniform or quasi-uniform flow. To this end, in Section 2, references are made to the methods used for the calculation of the free surface profiles in open-channel flow and to the different drag coefficient predictors, with particular emphasis on the approach proposed by Wang et al. [1]. Thus, Section 3 illustrates the equipment used to perform the experiments in the presence of rigid and emergent vegetation (simulated with cylindrical wooden sticks). In Section 4, considering 26 experimental profiles with linear patterns, the results of both literature predictors and the methodology proposed by Wang et al. [1] are shown. When following the approaches proposed by these authors, the relationship between drag coefficient and Reynolds number appears to be puzzling, showing in some cases a maximum and a minimum value, and in some other cases increasing or decreasing linear trends. To solve this problem, first of all, the experimental profiles were simulated, each one with the appropriate Manning coefficient, to compute the relevant drag coefficient. Dimensional analysis was then applied to obtain, from data for 16 experimental tests, a relationship allowing the drag coefficients to be estimated. Afterwards, the ability of the equation to simulate the experimental profiles was verified for the whole group of 26 linear patterns. The results were very accurate. Good results were also obtained in the simulation of profiles related to four experimental tests of Wang et al. [1]. By contrast, when the equation was used for three tests with staggered patterns the results were unsatisfactory, because of the different wake structure. Finally, Section 5 draws the conclusions of the present study.

2. Theory and Literature Predictors for the Drag Coefficient

2.1. Overview and Basic Definition

Very often, it is necessary to compute the free surface profile in an open channel for an assigned flow discharge. The main elements for the numerical calculation of the profile are summarized below, highlighting their peculiarities in the presence of emergent rigid vegetation. To this end, we refer to a GVF in a prismatic channel, where the energy grade line (EGL) slope can be locally evaluated using the equation for uniform flow with the relative coefficient of resistance and the local depth with an assumption that the flow is locally uniform.

From the Bernoulli equation, the total head, H, at any cross section can be determined as follows:

$$H = z_0 + h + \alpha \frac{V^2}{2g} \tag{1}$$

where z_0 is the bed elevation, h is the flow depth with respect to the channel bed, V is the mean flow velocity, α the kinetic energy flux correction factor and g is the gravitational acceleration. Differentiating Equation (1) with respect to the coordinate in the flow direction x, we obtain the following equation:

$$\frac{dH}{dx} = -J = -i + \frac{dE}{dx} \tag{2}$$

where J is the EGL slope, i is the bed slope (i.e., $i = -dz_0/dx$) and E $\left(E = h + \alpha V^2/(2g)\right)$ is the specific energy (usually, $\alpha = 1$).

In the numerical computation of the GVF profiles, the local J can be calculated from Manning's equation using the local flow depth, assuming that the flow is locally uniform [37]:

$$V = \frac{1}{n} R^{2/3} J^{1/2} \tag{3}$$

where n is the Manning coefficient and R is the hydraulic radius. For an open-channel flow without vegetation, n can be estimated from the channel bed and bank roughness. However, the roughness estimate becomes complicated in presence of vegetation elements.

Steady and locally uniform flow conditions require a local force balance between the flow driving the mechanism and the drag term. For a given length-scale dx along the streamwise direction, the flow driving mechanism is given by the component of the self-weight of the fluid along the flow direction, while the resistance is given by vegetation and the friction on the bottom and banks. Assuming that these latter can be neglected and considering a rectangular section, it is possible to obtain the following balance equation [1]:

$$\gamma B h dx \left(1 - \phi_{veg}\right) J = B dx F_D \tag{4}$$

where γ is the specific weight of the fluid, B is the cross-sectional width, ϕ_{veg} is the areal concentration of vegetation and F_D is the drag force exerted on vegetation per unit of area. Simplifying the terms that appear in Equation (4), one can write:

$$\gamma h \left(1 - \phi_{veg}\right) J = F_D. \tag{5}$$

If vegetation is simulated by rigid cylinders of diameter D, the resistance due to vegetation per unit riverbed area, spatially averaged, is given by the following equation:

$$F_D = \frac{1}{2} C_D m D h \rho U^2 \tag{6}$$

where C_D is the drag coefficient of the cylindrical vegetation, ρ is the fluid mass density and m is the number of vegetation stems per unit bed area, that is:

$$\phi_{veg} = m \pi D^2/4 \tag{7}$$

and U is the bulk velocity (or pore velocity), which is defined as follows:

$$U = \frac{Q}{B\left(1 - \phi_{veg}\right) h} \tag{8}$$

where Q is the flow discharge.

By replacing Equation (6) into Equation (5), one gets

$$J = \frac{C_D m D}{(1 - \phi_{veg})} \frac{U^2}{2g}. \tag{9}$$

On the basis of the above equations, the central role assumed by the drag coefficient in the calculation of the free surface profile is noticeable.

It should also be noted that the correct estimation of the drag coefficient is also important in the use of Reynolds Averaged Navier–Stokes (RANS)-based turbulence models [38,39] applied to flow in vegetated channel. In fact, in these models, the resistance due to vegetation is expressed through sub-grid forces that are added to the transport equations of turbulence and momentum, and, therefore, they require *a priori* the knowledge of the drag coefficient [40].

The analysis of different methods for estimating the drag coefficient described in Section 2.2 is limited exclusively to the case of emergent rigid vegetation when the flow does not affect the leaf apparatus. In the presence of real herbaceous vegetation, the drag coefficient is much lower than that in case of rigid vegetation [41], while it increases significantly when the flow affects the foliage [42–44]. It must be said, however, that foliage reconfiguration and inflection of the stems cause a reduction in the area of the affected plant and the drag exerted on it [45,46]. Jalonen and Jarvela [47] proposed a model in which the drags are considered separately when the flow affects both the trunk of the plants and their foliage.

It is also worth pointing out that some authors, in case of channels with emergent rigid vegetation, have directly focused on the Manning or Darcy–Weisbach coefficient instead of considering the dependence of the resistance to flow on C_D [48–50].

2.2. Existing Predictors of the Drag Coefficient

In the case of a single cylinder, the drag coefficient is a function of the Reynolds number, $Re_D = VD/\nu$, where ν is the kinematic viscosity of the fluid. Schlichting [51] proposed to estimate C_D as follows:

$$\begin{array}{ll} C_D = 3.07\, Re_D^{-0.168} & \text{for } Re_D < 800 \\ C_D = 1.0 & \text{for } 800 \le Re_D < 8000 \\ C_D = 1.2 & \text{for } 8000 \le Re_D < 10^5. \end{array} \tag{10}$$

Moreover, Cheng [52] suggested using the following equation:

$$C_D = 11 Re_D^{-0.75} + 0.9\left[1 - exp\left(-\frac{1000}{Re_D}\right)\right] + 1.2\left[1 - exp\left(-\left(\frac{Re_D}{4500}\right)^{0.7}\right)\right]. \tag{11}$$

When there is a set of cylinders, a mutual influence rises among them, owing to the strong interaction between the wakes and also between the cylinders and the wakes, especially when the vegetation density is high. In this way, the drag coefficient can be significantly different from unity. A number of studies were carried out in this regard.

The methods used to estimate the drag coefficient were based on theoretical analysis, on indirect or direct measurement, on the link with turbulence, on using computational fluid mechanics and on genetic programming. Some of the proposed formulas are recalled below and reference is made to Liu et al. [53], Sonnenwald et al. [54], D'Ippolito et al. [55,56] and Liu et al. [57] for a more extensive overview.

Li and Shen [58] analyzed the effects of different vegetation distributions on the resistance to flow and sediment transport. For the description of the flow field downstream of the cylinders that schematize the vegetation, they used the laws introduced by Petryk [59]. Considering $C_D = 1.2$ for a single cylinder, they determined the average asymptotic C_D associated with a number of cylinders, parallelly and alternately distributed, and at different mutual distances. As an example, with a distance among the cylinders equaling 10 times their diameter, and a channel slope of 0.002, they obtained an average C_D value of 1.1 in the

case of alternate distribution and 0.75 for a parallel-cylinder distribution. This is one of the few studies in which it was analyzed how the drag coefficient varies with the flow direction. The results obtained by Li and Shen [58] showed that the flow velocity is remarkably influenced by the cylinder number and the way they are spatially distributed. In particular, for a constant flow rate condition, the flow depth increases with the cylinders' number and depends on their spatial distribution. The flow depth increases with an increase in vegetation density, while the mean flow velocity and the shear stress at the walls decrease. Moreover, for constant flow rate and vegetation density, the flow depth is remarkably higher in case of alternate distribution with respect to the parallel one.

Later, Tanino and Nepf [60] proposed the following equation:

$$C_D = 2\left(\frac{\alpha_0}{Re_{D*}} + \alpha_1\right) \tag{12}$$

where α_0 is the contribution relative to the viscous forces on the cylinder surface, α_1 is the contribution from the inertial forces deriving by the pressure drop downstream of the cylinders, and $Re_{D*} = UD/\nu$. They found that α_1 varies linearly with the vegetation density, whereas α_0 is independent of the cylinder array characteristics for $\phi_{veg} > 0.15$.

Sonnenwald et al. [54], considering the literature data with square, staggered and random arrangements of the rigid cylinders, suggested the following equation:

$$C_D = 2\left(\frac{6475D + 32}{Re_{D*}} + 17D + 3.2\phi_{veg} + 0.5\right) \tag{13}$$

where the coefficients of the D terms have units of m^{-1} to preserve the non-dimensionality.

Cheng and Nguyen [61] introduced, under the hypothesis that the wall and bottom effects are negligible, the vegetation-related hydraulic radius, r_v, which takes into account the density and the diameter of the vegetation, as $r_v = (\pi/4)\left(\left(1 - \phi_{veg}\right)/\phi_{veg}\right)D$. Thus, they defined the vegetation Reynolds number as $Re_v = Ur_v/\nu$. Using the experimental data from several authors (random and staggered distributions and only two linear cases), Cheng and Nguyen [61] showed that the drag coefficient decreases monotonically with an increase in Re_v and proposed the following equation:

$$C_D = \frac{50}{Re_v^{0.43}} + 0.7\left[1 - exp\left(-\frac{Re_v}{15,000}\right)\right]. \tag{14}$$

An estimate of the drag coefficient, using the direct measurements, was performed by Ishikawa et al. [62], Kothyari et al. [11] and D'Ippolito et al. [63], among others. In Ishikawa et al. [62], the cylinders were distributed on a grid with a staggered pattern forming angles of 45° with the flow direction and the action was calculated averaging the values obtained for 7 or 13 cylinders. In Kothyari et al. [11], the angle formed with the flow direction was 30° and the action was determined on only one cylinder. Instead, D'Ippolito et al. [63] used a linear arrangement of the cylinders and the action was calculated as the mean of that exerted on a cylinder group from 2 to 25.

In the experiments of Ishikawa et al. [62], the drag coefficients differ significantly for the same stem Reynolds number, although the dependence is unclear. They provided three equations for the drag coefficient as a function of the areal density, depending on the flume bottom slope.

In Kothyari et al. [11], the density ϕ_{veg} ranges between 0.0022 and 0.0885. For a subcritical flow, they obtained the following equation:

$$C_D = 1.53\left[1 + 0.45ln\left(1 + 100\phi_{veg}\right)\right]Re_{D*}^{-3/50} \tag{15}$$

in which C_D remarkably increases with ϕ_{veg} and slightly varies with Re_{D*}.

D'Ippolito et al. [63], on the basis of 70 tests with emerging stems in a linear arrangement, in uniform or quasi-uniform flow conditions, proposed an equation in which C_D is a function of the density ϕ_{veg} only:

$$C_D = 0.211ln(100\phi_{veg}) + 0.784. \quad (16)$$

The equation is valid for ϕ_{veg} from 0.003 to 0.05, i from 0.48% to 2.02% and Re_{D*} from 1000 to 10,000. The values obtained from Equation (16) are smaller than those obtained from Equation (15) for a given ϕ_{veg}, owing to the two different cylinders arrangements (a triangular mesh in the case of Kothyari et al. [11] and a square mesh in the case of D'Ippolito et al. [63]).

Nepf [64] assumed that the production of turbulence in the presence of vegetation is equal to the dissipation and that the turbulent intensity is equal to the drag forces.

Liu et al. [57] utilized genetic programming to develop a predictor of drag coefficients from the experimental data. They did not take into account the influence of the arrangement of the cylinders and expressed the drag coefficient as a function of Re_{D*}, ϕ_{veg} and the blockage ratio ψ. This latter, defined as $\psi = D/L_y$, where L_y is the lateral distance between adjacent stems at the same streamwise location, reflects the blockage effect on a multi-cylinder array. Liu et al. [57] employed 475 data points relative to random and staggered cylinder distributions. Among all the solutions provided by the software Eureqa, Liu et al. [57] selected the final expression of C_D that could balance the complexity, accuracy and physical meaning to a great extent:

$$C_D = \frac{189}{Re_{D*}} + 0.82 + \psi^2 + 6.02\phi_{veg}. \quad (17)$$

This expression has the same form as Equation (12) with the term α_1 function of the blockage factor and density.

Lama et al. [65], in the evaluation of flow resistance models based on field experiments in a partly vegetated reclamation channel, considered $C_D = 1$.

The above drag coefficient estimates are based on the experiments carried out under the conditions of uniform or quasi-uniform flow. More recently, the drag coefficient (or Manning coefficient) variation along the flow direction was also analyzed in the case of non-uniform steady flow.

Yerdelen et al. [66] calculated the drag coefficient on the basis of approximately 70 experiments under the assumption of uniform and non-uniform steady flows. These authors stated that adopting the C_D values obtained under the conditions of uniform flow, when the flow is not uniform, leads to significant errors and, moreover, by excluding the smallest densities ($\phi_{veg} = 0.3\%$), the drag coefficient decreases with an increase in Re_D. It should be noted that they referred to the average values collected in the field.

Wang et al. [1] analyzed the influence of vegetation on the non-uniform steady flow profile in the absence of a strong driving gradient. They observed eight M2 type profiles on a flume with $i = 0\%$, in vegetated section of lengths L between 0.52 and 0.67 m with densities between 1% and 41.9%. The flow rate was constant with $Q = 3.84 \times 10^{-3}$ m^3 s^{-1}, while the upstream flow depths h_0 were between 4.7 and 21 cm and the cylinder diameter $D = 1$ cm. The numerical simulation of the profile, carried out from upstream, resulted in an overestimation of the measured water depth when the drag coefficient was calculated with the equation for a single cylinder (Equation (11)). Instead, using the equation that takes into account the mutual influence of the cylinders (Equation (14)), the water depth was underestimated in the case of high vegetation density and overestimated for a low vegetation density. They, therefore, searched for an alternative expression to represent the drag coefficient. The measured water depth h as a function of the distance x from the beginning of the vegetated part of the channel was smoothed with the following mathematical function:

$$h = c_1 ln|x - c_2| + c_3 \quad (18)$$

where the constants c_1, c_2 and c_3 were determined with the Matlab software (The MathWorks, Inc., Natick, Middlesex County, MA, USA). Having obtained the average flow profiles, Wang et al. [1] computed the local drag coefficient C_D by means of Equation (8). They observed a non-monotonic pattern of the drag coefficient C_D versus the stem Reynolds number Re_{D*}; indeed, the C_D increases from the inlet (low Re_{D*}), reaching a peak value, and then decreases toward the outlet (high Re_{D*}). Starting from Equation (2), Wang et al. [1] proposed the following equation:

$$C_{D-W} = \frac{2g(1-\phi_{veg})}{mD}[P^* - A^*] \tag{19}$$

where P^* and A^* represent the advection and pressure components, respectively, and are functions of Re_{D*}. Specifically, the two terms can be calculated as follows:

$$P^* = S_h D^2 \nu^{-2} Re_{D*}^{-2} \tag{20}$$

and

$$A^* = \frac{S_h B \nu (1-\phi_{veg})}{gQD} Re_{D*} \tag{21}$$

where S_h is the free surface slope, which can be determined from

$$S_h = -\frac{\partial h}{\partial x} = c_1 exp\left[\frac{c_1}{c_2} - \frac{QD}{c_1 B \nu (1-\phi_{veg})} Re_{D*}^{-1}\right]. \tag{22}$$

Wang et al. [1] showed how P^* and A^* explain the non-monotonic behavior of C_D along x for the experiments with $0.01 \leq \phi_{veg} \leq 0.419$ and also how, in the specific case of a constant flow discharge, the coefficients c_1 and c_1/c_2 depend on ϕ_{veg}, while c_3 depends on c_1, c_2 and the flow depth in the upstream cross section. In case of Wang's et al. [1] experiments, characterized by $i = 0$, Equation (19) introduced into Equation (2) allows the detected profiles to be reproduced in a quite correct way.

3. Experimental Data

A series of experiments was carried out at the "*Laboratorio Grandi Modelli Idraulici*" of the Department of Civil Engineering, University of Calabria, Italy. We used a hydraulic flume (11.13 m long), with the bottom made of PVC, of width $B = 0.382$ m and plexiglass walls (0.21 m high) set on a reticular beam (Figure 1). The beam was sustained by two crossbars, of which the one downstream was linked with a hinge to the beam, so that the flume could be put at the desirable slope. A small caisson sustained by the same beam, 104 cm long and with the same cross-section as the flume, upstream of this one and fed by the laboratory constant-level tanks, was equipped with calm-grids and allowed its entrance into the water without any disturbance.

A valve on the input pipe allowed the flow rate regulations, and its measurement was possible by means of a Thomson weir downstream of the flume outlet. The vegetation was modeled by means of two sets of small wooden circular cylindrical rods ($D = 0.8$ and 1.0 cm) placed in a central portion of the flume (starting at x = 630 cm from the inlet) of variable length, approximately between 1.5 and 2.2 m. The rods were perpendicular to the bottom of the flume and were secured to two wooden box-structured plates. In a previous study [63], the drag forces acting on a group of stems were measured by maintaining the stem ends at a distance of about 1 mm from the bottom in uniform or quasi-uniform flow conditions.

In this study, 29 free surface profiles were observed, with four stem densities, achieved arranging the stems on three square meshes (D4, D5, D9) at two distances, $\Delta x = \Delta y = s = 4.24$ and 8.48 cm, where Δx and Δy are the spatial distances between the centers of two stems in the streamwise and spanwise directions, respectively, and one staggered mesh (D4–5). The four arrangements are sketched in Figure 2. Three different

bed slopes were considered, $i_1 = 0.48\%$, $i_2 = 1.35\%$, $i_3 = 2.02\%$, and the flow rate was varied between 5.27×10^{-3} and 16.39×10^{-3} m^3/s.

Figure 1. Hydraulic flume.

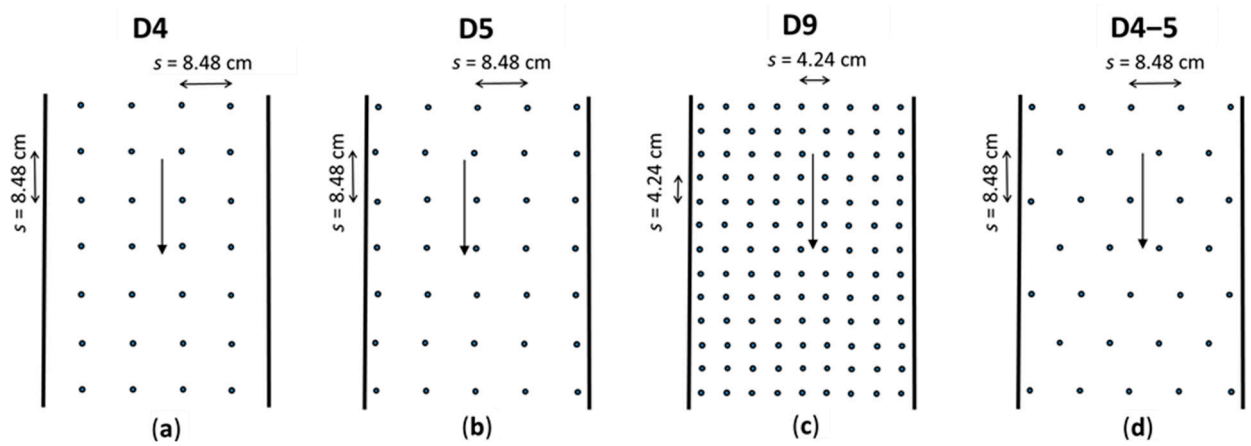

Figure 2. Stem arrangements: (**a**) D4; (**b**) D5; (**c**) D9; (**d**) D4-5.

As for the water level reading, we adopted the following procedure. Once the flume was set on the horizontal, the cross-section downstream was closed by a small penstock and the water was entered into the flume up to a depth of 3 cm. On the wall at the right side, some metric scales were put, drawn onto transparent plastic sheets, at a distance of 1 m from each other. The metric scales were then adjusted to the free water surface. Since previously the flume bottom was carefully levelled, the metric scale reading gave the water depth. In the flume reach with the stems, the metric scales were closer to each other. The average water level in cross-sections was obtained by watching through the transparent metric scales. The flume reaches from upstream, and downstream the stems presented cross-sections with a practically horizontal water surface, even though the flow had waves of amplitude 1 to 2 mm. In the reach equipped with the stems, the flow was approximately steady, presenting regular patterns of crests and hollows, so that the measurement by means of digital instruments or more refined techniques only apparently would have given better results, without any insight. In some cases, the water profiles were checked by means of photographs with good results.

The experiments showed M2 or M3 − M2 free surface profiles. At the end of the stems array, we could observe, in many cases, the critical depth $h_c = \sqrt[3]{q^2/g}$, where q is the flow rate per unit bed width ($q = Q/B$). In some cases, even with a M2 profile, a depth higher than the critical one was imposed downstream by means of a plate rotating around a hinge at the channel bottom. When a M3 profile was found upstream and a M2 profile downstream, a hydraulic jump was observed between the two. Table 1 provides a summary

of the experimental parameters, where the vegetation density is expressed as the number of stems present on a row multiplied with the area of one stem and divided by the area of influence (sB).

Table 1. Characteristic parameters and results of the experiments.

Test n.	Arrangement	Q (L/s)	i (%)	d (mm)	ϕ_{veg} (%)	Profile Type
T1	D9	13.55	2.02	10	4.36	M2
T2	D9	16.39	2.02	10	4.36	M2
T3	D9	7.90	1.35	10	4.36	M2
T4	D9	10.96	1.35	10	4.36	M2
T5 [1]	D9	13.77	1.35	10	4.36	M2
T6	D5	16.31	2.02	10	1.21	M3-M2
T7	D4	10.96	1.35	10	0.97	M3-M2
T8	D9	8.6	2.02	8	2.79	M2
T9	D5	10.92	1.35	10	1.21	M3-M2
T10	D9	5.29	1.35	10	4.36	M2
T11 [1]	D9	14.62	0.48	8	2.79	M2
T12	D9	5.77	2.02	8	2.79	M2
T13	D4-5	7.7	0.48	8	0.63	M2
T14	D4-5	13.2	0.48	8	0.63	M2
T15	D4-5	17.4	0.48	8	0.63	M2
T16	D4	16.31	2.02	10	0.97	M3-M2
T17	D9	5.27	2.02	10	4.36	M2
T18	D9	7.87	2.02	10	4.36	M2
T19	D9	10.86	2.02	10	4.36	M2
T20	D9	7.99	0.48	10	4.36	M2
T21	D5	13.77	1.35	10	1.21	M2
T22	D4	13.77	1.35	10	0.97	M3-M2
T23 [1]	D9	7.99	1.35	10	4.36	M2
T24	D9	13.77	1.35	10	4.36	M2
T25	D5	13.88	2.02	10	1.21	M3-M2
T26 [1]	D9	14.53	1.35	8	2.79	M2
T27 [1]	D9	11.61	0.48	8	2.79	M2
T28	D9	11.55	2.02	8	2.79	M2
T29	D9	14.62	2.02	8	2.79	M2

[1] Experiments in which a plate was placed at the end of the channel allowing the adjustment of the flow depth.

4. Results and Discussion

4.1. Drag Coefficient Predictors Performance

Even though not all the literature equations cited in Section 2.1 have been applied to the experimental data of the present study, five of them, Sonnenwald et al. [54], Cheng and Nguyen [61], Kothyari et al. [11], D'Ippolito et al. [63] and Liu et al. [57], gave us the results with a C_D value ranging between 0.77 and 1.73. Unfortunately, the representation of the computed C_D values versus the experimental ones (derived from Equation (9), using experimental data for J, ϕ_{veg}, m, D, U) is not satisfactory, as shown in Figure 3.

In detail, each of these equations shows a narrow range in predicted values, which appear scarcely correlated with the experimental data. This behavior could be attributed to the origin of the predictor equations, mainly derived from the uniform or quasi-uniform flow conditions, and difficult to adapt to the GVF conditions, which is the object of the present study.

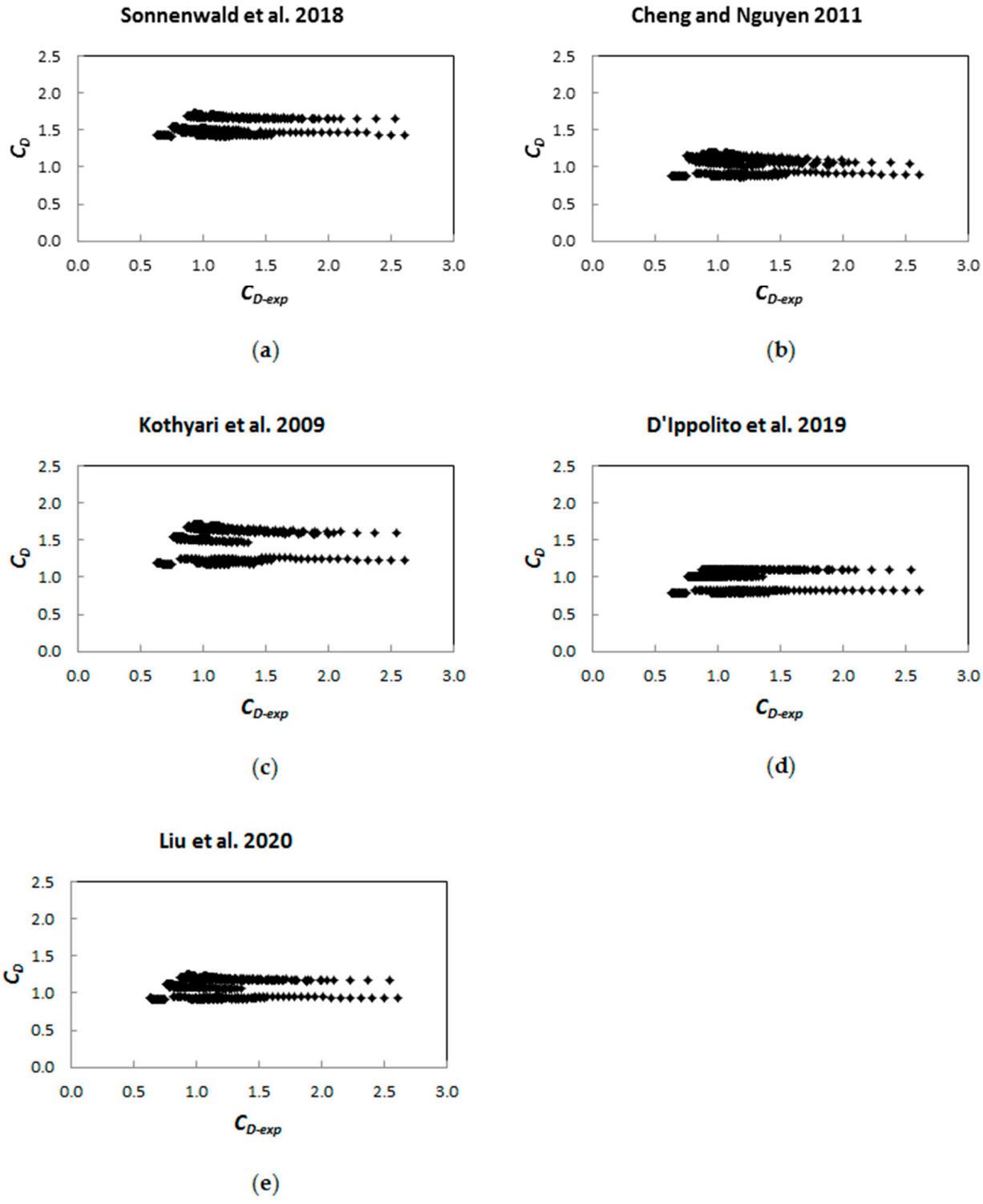

Figure 3. Comparison between the calculated and observed C_D values using different predictors. (**a**) Sonnenwald et al. [54], Equation (3); (**b**) Cheng and Nguyen [61], Equation (14); (**c**) Kothyari et al. [11], Equation (15); (**d**) D'Ippolito et al. [63], Equation (16); (**e**) Liu et al. [57], Equation (18).

4.2. Wang et al. (2015) Procedure

The above consideration can also be extended to Wang et al.'s [1] procedure. First, we used the same method as Wang et al. [1] to determine how the drag coefficient varies in the flow direction. In particular, the c_1, c_2 and c_3 values of Equation (18) that best represented

the experimental profile were determined for each test. Figure 4 shows for tests T5 and T18, the experimental points and the profiles obtained with Equation (18).

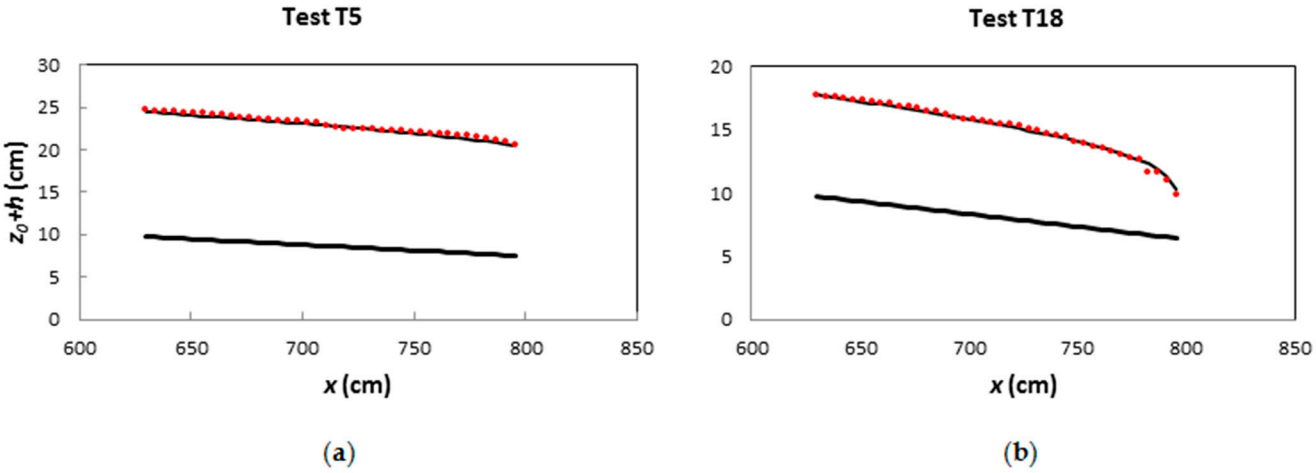

Figure 4. Comparison between the measured flow depth and the fitted logarithmic function [1]: (**a**) T5; (**b**) T18. The black bold line indicates the flume bottom; the black line is the calculated free surface; the red symbols indicate the measured free surface.

Considering the calculated flow depths, it was possible to determine the EGL slope and, subsequently, the values of the drag coefficients using Equation (9) (here identified as C_{D-W}). Some results are shown in Figure 5.

While in the experiments of Wang et al. [1] the trends of C_D as a function of Re_{D*} were parabolic, in the present study, they were much more complex, showing in some cases a maximum and a minimum value, and in others increasing or decreasing linear trends. In particular:

1. the M2 profiles that start from the critical depth have a bell-shaped pattern, at least on one side (T1, T3, T4, T17, T18, T24), and in some cases rather flat (T2, T19, T29). The difference, compared to the trends of Wang et al. [1], is probably accredited to the fact that in those experiments the flume bed was horizontal;
2. when the bell is narrow, i.e., the variation in Re_{D*} is about 1000–2000, there is, on the left, an increase in C_D as Re_{D*} decreases (T7, T9, T10, T21, T22, T28);
3. when there is a hydraulic jump in the profile (M3-M2), the C_D value decreases as the Re_{D*} increases (T6, T16, T25);
4. if the test was performed by inserting the plate at the end of the channel (i.e., with a flow depth, downstream of the flow, higher than the critical one), the trend of C_D slightly increases with Re_{D*} (T5, T11, T20, T27) or remains almost constant (T23, T26).

These conditions made it difficult to find a general law for C_D and encouraged us to try in a different way.

4.3. A New Method to Compute the Average Free Surface Profile

We start by considering that using the traditional Manning equation, it is possible to determine the average value of the EGL slope, J_a, as follows:

$$J_a = \frac{n^2 U_a^2}{R_a^{4/3}} \tag{23}$$

where U_a and R_a are the average values of velocity and hydraulic radius, respectively. For a fixed value of n, the free surface profile can be calculated using the direct step method [37]. In fact, if a downstream flow depth is known, an upstream one can be fixed and the

distance between the two relative sections, Δx, can be calculated using the finite difference of Equation (2), that is:

$$\Delta x = \frac{\Delta E}{i - J_a} \tag{24}$$

with J_a given by Equation (23) and where ΔE is the difference between the downstream and upstream specific energies.

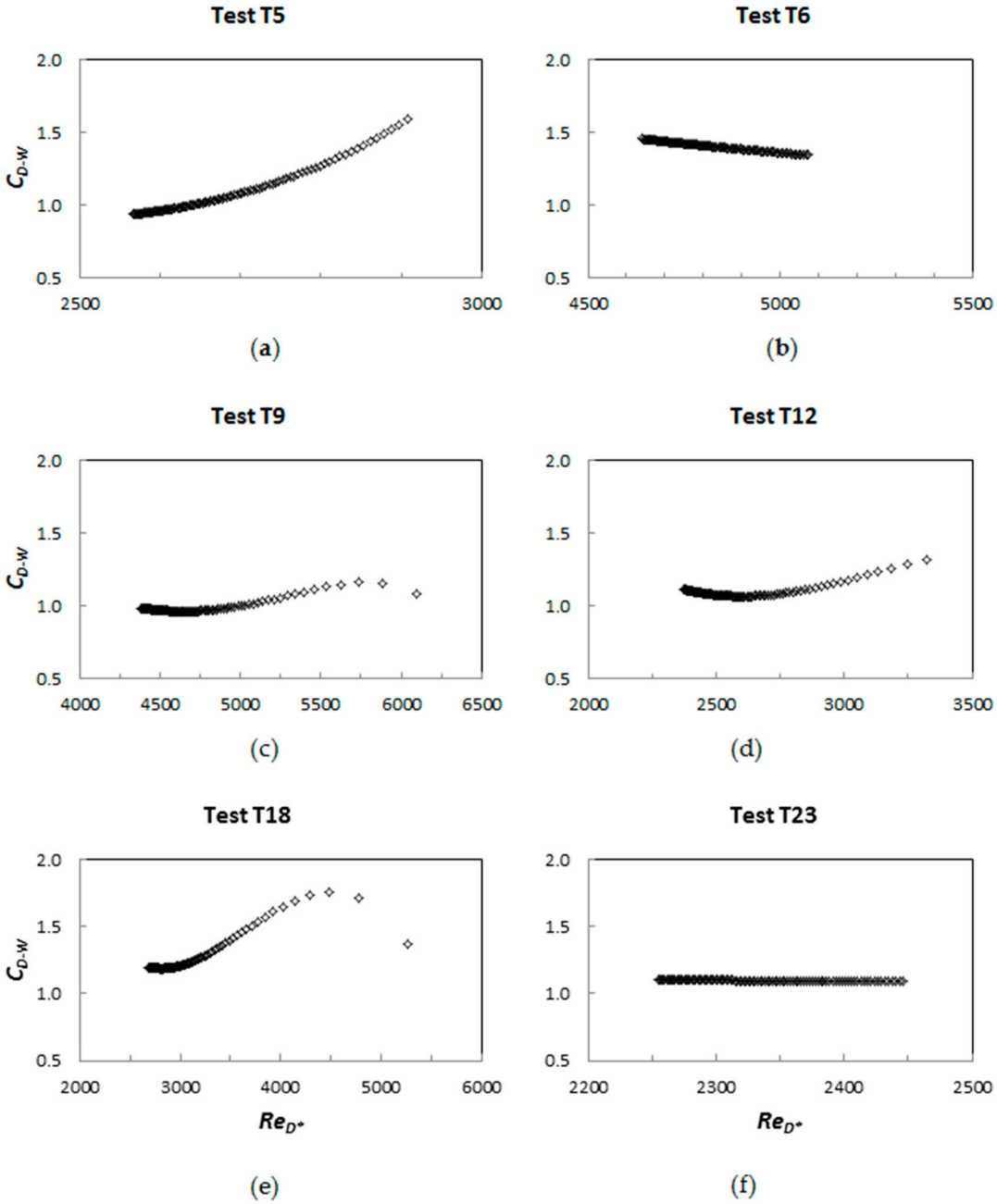

Figure 5. Drag coefficients obtained following the procedure of Wang et al. [1]: (**a**) T5; (**b**) T6; (**c**) T9; (**d**) T12; (**e**) T18; (**f**) T23.

The direct step method permits the identification, for each test, of the n value that best allows the experimental free surface profile to be reproduced. As an example, Figure 6 shows for tests T5 and T18 the comparison between the calculated and measured free surface profiles, with the corresponding n values that best represent them.

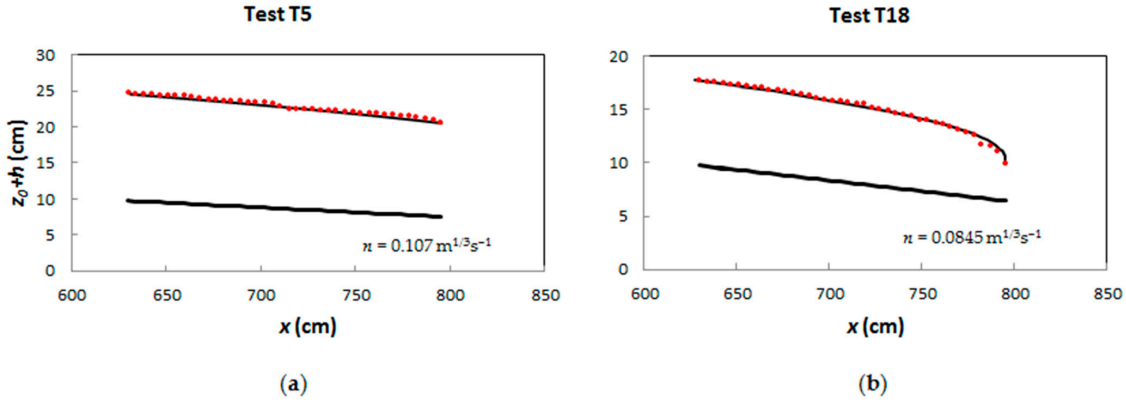

Figure 6. Comparison between the measured and the calculated free surface profiles obtained by means of the best Manning coefficient: (**a**) T5; (**b**) T18. The black bold line indicates the flume bottom; the black line is the calculated free surface; the red symbols indicate the measured free surface.

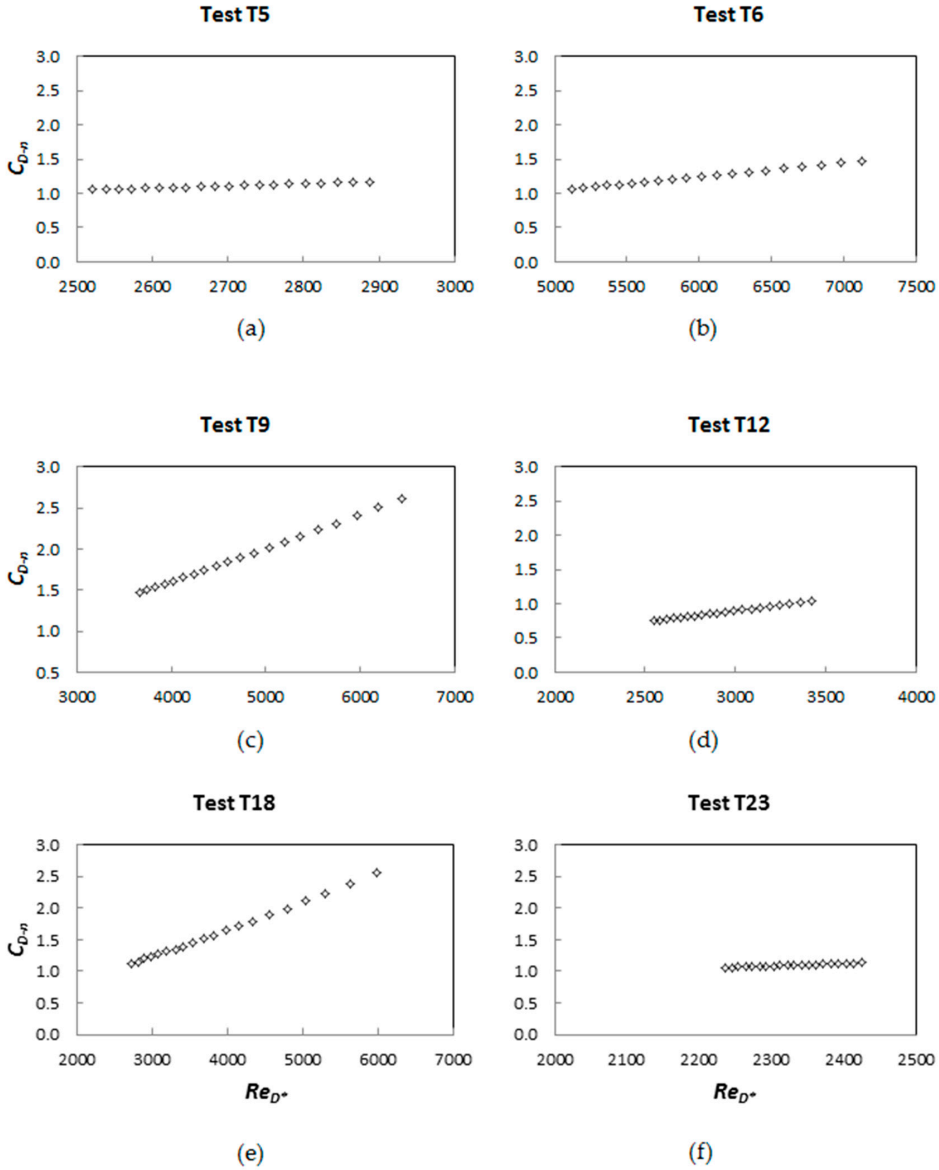

Figure 7. Drag coefficients C_{D-n} computed by means of the best Manning coefficient versus Re_{D*}: (**a**) T5; (**b**) T6; (**c**) T9; (**d**) T12; (**e**) T18; (**f**) T23.

In this way, we obtained a continuous line representing the free surface profile and the J values for each abscissa. The C_D experimental values, here identified as C_{D-n}, were computed by means of Equation (9) and, when plotted versus Re_{D*}, they appear as in Figure 7.

In each subplot, C_D presents a monotonic pattern versus Re_{D*}, with the maximum value at the end of the stem array, where the maximum value of Re_{D*} was found.

4.4. Dimensional Analysis and Regression Equation for C_D

Considering a squared arrangement of cylinders in an element of bed with emergent vegetation and looking at Figure 2, we assumed D, s, h, ϱ, g, v and U as independent variables, and F'_D, drag force exerted on the stems per unit bed area, as a dependent variable.

Thus, we obtained the following relationship:

$$F'_D = \psi_F(D,\ s,\ h,\ \rho, g,\ \nu, U) \tag{25}$$

being ψ_F a generic function. By means of dimensional analysis, we obtained:

$$\frac{F'_D}{\rho U^2} = \psi_F\left(\frac{s}{D},\ \frac{h}{D},\ Fr_D,\ Re_{D*}\right) \tag{26}$$

where $Fr_D = U/\sqrt{gD}$, that is the stem Froude number. Since it is possible to assume only one non-dimensional parameter between Fr_D and Re_{D*}, the drag coefficient can be expressed as follows:

$$C_D = \psi(\phi_{veg},\ Re_h,\ Re_{D*}) \tag{27}$$

where $Re_h = Uh/\nu$, that is the flow Reynolds number with a characteristic length h. One can observe that $Uh = q$ remains constant along a given free surface profile. To try and find a regression equation for C_D, among the 26 tests with a linear arrangement, we considered the following 16: T1, T2, T3, T4, T6, T7, T10, T11, T17, T18, T19, T21, T24, T25, T27, T29.

Figure 8 shows the C_D values (here identified as C_{D-n}) versus Re_{D*}.

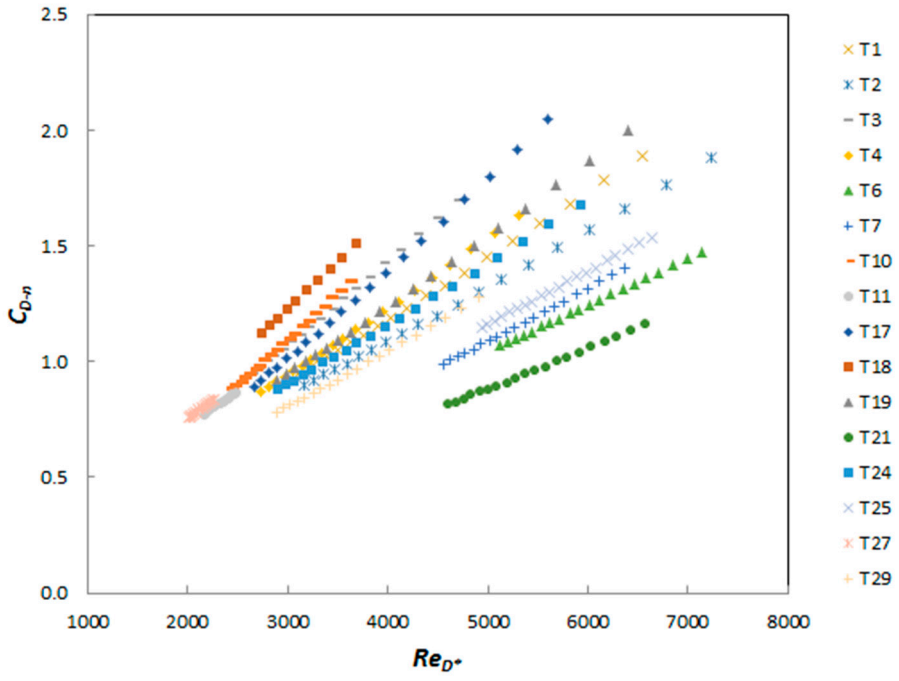

Figure 8. Drag coefficients C_{D-n} computed by means of the best Manning coefficient versus Re_{D*} for 16 experiments.

The pattern of C_D is, in practice, linear with Re_{D*}. Since from the dimensional analysis we obtained Equation (27) by means of a regression analysis, we can define the following linear equation:

$$C_{D-UC} = 10.83\phi_{veg} + 0.2043\,\frac{Re_{D*}}{1000} - 0.0675\frac{Re_h}{10,000} + 0.1765 \tag{28}$$

where C_{D-UC} stands for University of Calabria drag coefficient with a determination coefficient R^2 = 0.83. Figure 9 shows the computed C_{D-UC} values versus the experimental ones (16 tests with 310 values of the drag coefficient were considered; few points of test T18 were not included because they were, probably, affected by measurement errors). Equation (28) shows that, as expected, C_{D-UC} increases with ϕ_{veg} and Re_{D*} and decreases with Re_h; this equation gives a maximum error of 20%, even though most of the points lay into the 10% error band (Figure 9).

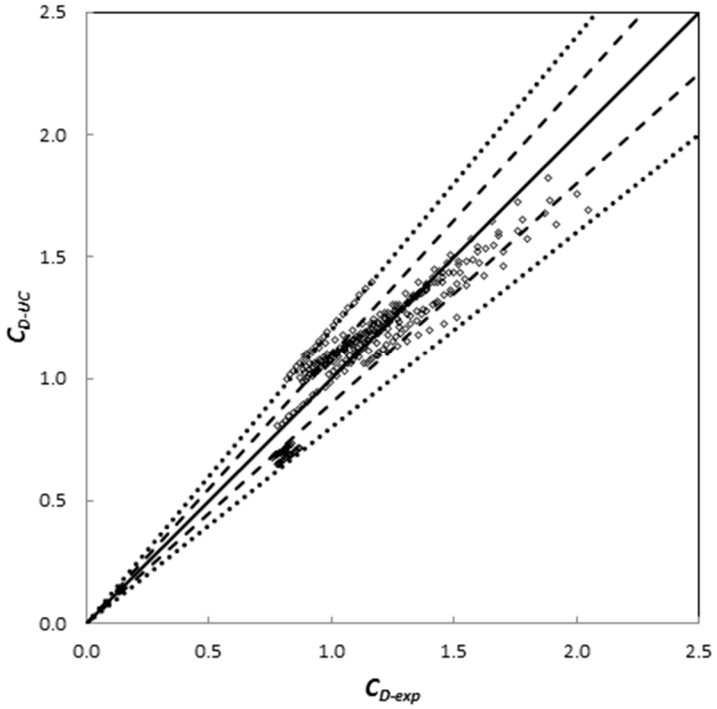

Figure 9. Comparison of the computed C_{D-UC} values using Equation (28) vs. the experimental ones. The dashed lines indicate an error equal to ±10%; the dotted lines indicate an error equal to ±20%.

4.5. Calculation of the Free Surface Profiles in Linear Arrangement

Equation (2) allowed simulation of free surface profiles, once again by the direct step method and adopting the C_{D-UC} values. The new profiles fit very well the experimental $(x,\ z_0 + h)$ points. As an example, Figure 10 shows the results for tests T1, T5, T8, T9, T18 and T23. Note that profiles T5, T8, T9 and T23 were not used in the determination of Equation (28), because they were used for validating it.

Equation (28) was also used to simulate four of the profiles observed by Wang et al. [1], i.e., the ones with comparable densities (Φ_{veg} = 1.0%, 1.8%, 4.1% and 7.3%) to those for which the above equation was derived (Φ_{veg} = from 0.97% to 4.36%). The comparisons between the experimental and simulated profiles for two densities are shown in Figure 11. Both profiles are well simulated, whereas the water depth related to densities Φ_{veg} = 1.8% and 4.1% is slightly underestimated. It should be pointed out that Equation (1) was derived from the results of experimental tests relating to slopes 0.48% < i < 2.2%. Thus, we can conclude that the method here proposed can give good results.

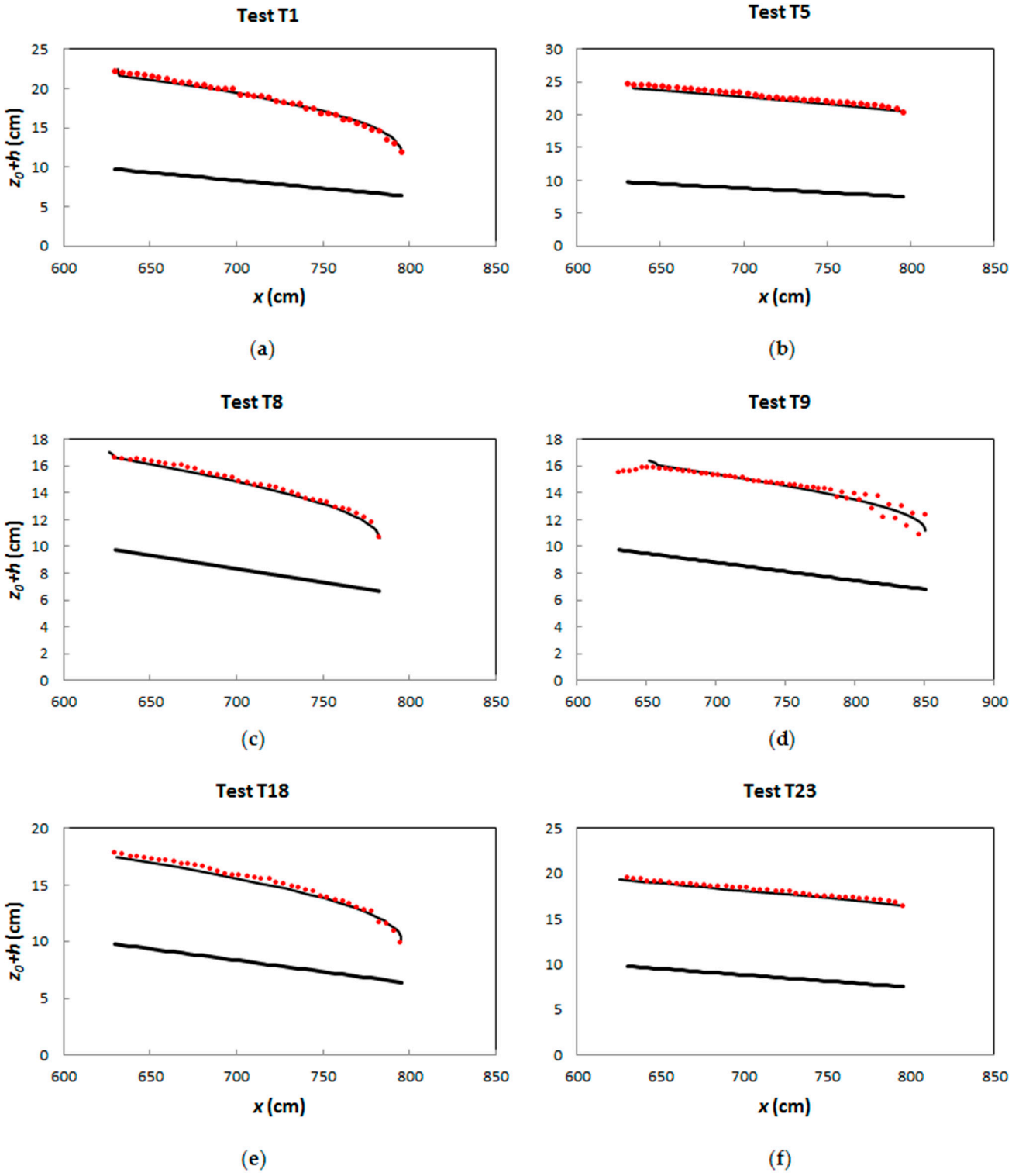

Figure 10. Comparison between the measured and the calculated free surface profiles obtained using C_{D-UC}: (**a**) T1; (**b**) T5; (**c**) T8; (**d**) T9; (**e**) T18; (**f**) T23. The black bold line indicates the flume bottom; the black line is the calculated free surface; the red symbols indicate the measured free surface.

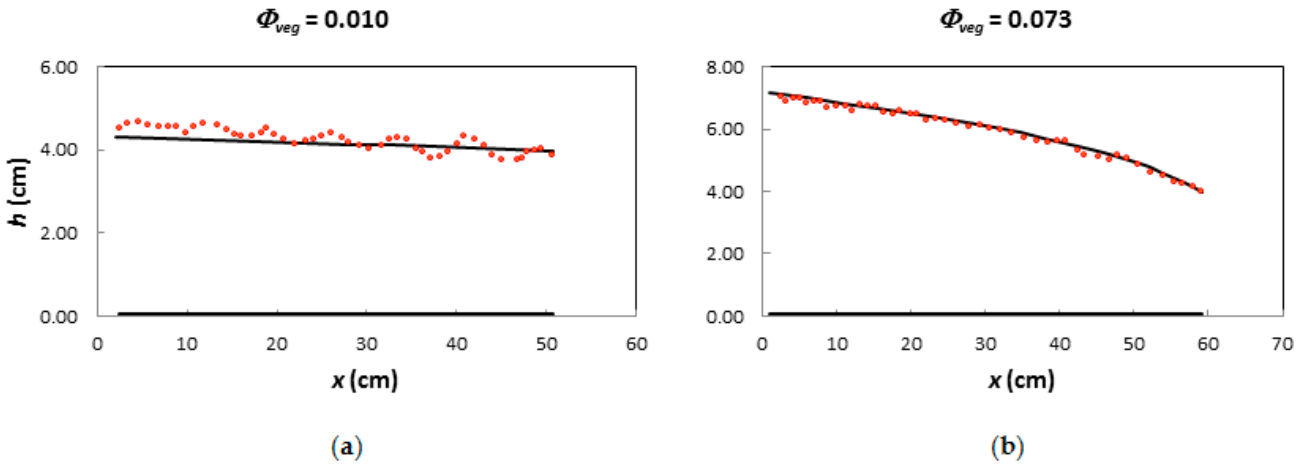

Figure 11. Comparison between two free surface profiles measured by Wang et al. [1] and the profiles calculated using C_{D-UC}: (**a**) $\phi_{veg} = 0.01$; (**b**) $\phi_{veg} = 0.073$. The black bold line indicates the flume bottom; the black line is the calculated free surface; the red symbols indicate the measured free surface.

4.6. Calculation of the Free Surface Profiles in the Staggered Pattern

Wang et al. [1] applied their relationship for estimating the drag coefficient (derived for the case in which the cylinders were arranged according to a linear distribution) to a test in which the cylinders were arranged according to a diagonal distribution. The obtained profile showed a satisfactory agreement between the measured and calculated results, such that Wang et al. [1] argued that the model results were insensitive to the precise vegetation arrangements.

Similarly, we tested Equation (28), derived in the case of a linear distribution, on the three tests T13, T14 and T15, which were carried out with a staggered pattern, with a lower density.

The obtained results showed that the flow depths are significantly underestimated. Figure 12 shows the experimental and calculated free surface profiles with reference to two different flow rates $Q = 7.7 \times 10^{-3}$ and 17.4×10^{-3} m^3/s (tests T13 and T15, respectively).

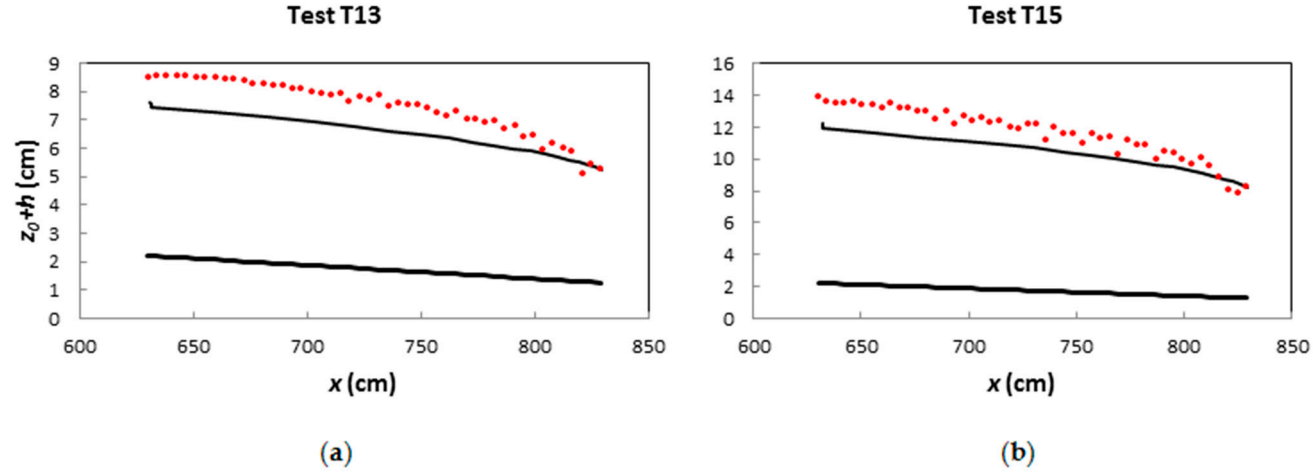

Figure 12. Comparison between the measured and the calculated free surface profiles obtained using C_{D-UC} in the case of staggered pattern: (**a**) T13; (**b**) T15. The black bold line indicates the flume bottom; the black line is the calculated free surface; the red symbols indicate the measured free surface.

Thus, Figure 12 shows that, according to Schoneboom et al. [67] for tests under uniform flow conditions, for similar vegetation densities and boundary conditions a staggered

vegetation distribution results in a higher resistance, and thus a higher drag coefficient than that of a linear vegetation distribution. As also observed by Schoneboom et al. [67], this depends on the different structure of turbulent wakes.

5. Conclusions

The vegetation along watercourses has an important impact from a hydrodynamic viewpoint because it increases the flow resistance. In the case of rigid vegetation, the drag coefficient is usually used to represent this resistance. In the literature, many formulas were proposed according to different methodologies that take into account, among other variables, the vegetation density, its arrangement, the stem diameter and the Reynolds number, which are computed by taking a characteristic length as the hydraulic radius relative to the vegetation or the vegetation stem diameter. These formulas were derived either by reference to uniform or quasi-uniform flow, or by reference to a small number of cylinders in which the flow depth varies very slightly. Recently, Wang et al. [1], considering a horizontal bed flume, analyzed how the drag coefficient varies in the flow direction. Wang et al. [1] discovered that the drag coefficient has a parabolic trend in the streamwise direction. The same methodology applied to 26 experimental free surface profiles observed at the University of Calabria, with the bottom characterized by small or medium slopes showing, instead, a different behavior. Indeed, the drag coefficient values had a puzzling trend with the Reynolds number, in some cases with maximum and minimum values, and in others cases with increasing or decreasing linear trends. After simulating the observed profiles by means of appropriate Manning coefficients, we computed drag coefficients that showed a linear trend with the Reynolds number (evaluated with the flow depth). On the basis of dimensional analysis, in the case of a square arrangement, the variables influencing the drag coefficient were derived, that is the density of the vegetation and the two Reynolds numbers computed using the characteristic lengths as the flow depth or the cylinders' diameter. A regression equation was derived from the results of 16 tests and used to reproduce all the 26 experimental profiles. The results were quite satisfactory. Good results were also obtained in simulating the experimental tests of Wang et al. [1] with comparable density. Thus, the new equation can be used in the range of values investigated in this study and in the case of square vegetation arrangements. Indeed, its application to a staggered distribution showed that the flow depths are underestimated and, therefore, cannot be applied in such cases.

Author Contributions: Conceptualization, F.C., S.D., R.G. and A.D.; formal analysis, A.D. and N.P.; writing—review and editing, A.D. and N.P.; supervision, F.C., S.D. and R.G.; funding acquisition, F.C. and R.G. All authors have read and agreed to the published version of the manuscript.

Funding: This research was funded by the "SILA" PONa3_00341 project, "An Integrated System of Laboratories for the Environment".

Data Availability Statement: The data presented in this study are available on request from the corresponding author.

Conflicts of Interest: The authors declare no conflict of interest.

References

1. Wang, W.J.; Huai, W.X.; Thompson, S.; Katul, G.G. Steady nonuniform shallow flow within emergent vegetation. *Water Resour. Res.* **2015**, *51*, 10047–10064. [CrossRef]
2. Peel, M.C. Hydrology: Catchment vegetation and runoff. *Prog. Phys. Geog.* **2009**, *33*, 837–844. [CrossRef]
3. D'Ippolito, A.; Ferrari, E.; Iovino, F.; Nicolaci, A.; Veltri, A. Reforestation and land use change in a drainage basin of Southern Italy. *iForest* **2013**, *6*, 175–182. [CrossRef]
4. Bombino, R.; Pérez-Cutillas, P.; D'Agostino, D.; Denisi, P.; Labate, P.; Martínez-Salvador, A.; Zema, D.A.; Zimbone, S.M.; Conesa-García, C. Comparing the hydrological response of regulated vs. unregulated forested headwaters in the Mediterranean semi-arid environment. *Water* **2021**, *13*, 1275. [CrossRef]
5. Iovino, F. *La Ricostruzione Boschiva in Calabria. Modello di Riferimento del Passato con Approcci Attuali in Tema di Tutela del Territorio e Dell'ambiente*; Rubbettino Editore: Soveria Mannelli, Italy, 2021. (In Italian)

6. Wang, H.; Tang, H.W.; Yuan, S.Y.; Lv, S.Q.; Zhao, X.Y. An experimental study of the incipient bed shear stress partition in mobile bed channels filled with emergent rigid vegetation. *Sci. China Technol. Sci.* **2014**, *57*, 1165–1174. [CrossRef]
7. Kazem, M.; Afzalimher, H.; Sui, J.Y. Characteristics of turbulence in the downstream region of a vegetation patch. *Water* **2021**, *13*, 3468. [CrossRef]
8. Coscarella, F.; Penna, N.; Ferrante, A.P.; Gualtieri, P.; Gaudio, R. Turbulent flow through random vegetation on a rough bed. *Water* **2021**, *13*, 2564. [CrossRef]
9. Derkhshan, S.; Afzalimher, H.; Singh, V.P. Effect of vegetation patch distribution on the flow resistance. *Int. J. Hydr. Eng.* **2021**, *10*, 19–25.
10. EU, Directive 2007/60/EC of the European Parliament and of the Council of 23 October 2007 on the Assessment and Management of Flood Risks. 2007. Available online: https://eur-lex.europa.eu/legal-content/EN/TXT/?uri=celex:32007L0060 (accessed on 20 April 2022).
11. Kothyari, U.C.; Hayashi, K.; Hashimoto, H. Drag coefficient of unsubmerged rigid vegetation stems in open channel flows. *J. Hydraul. Res.* **2009**, *47*, 691–699. [CrossRef]
12. Curran, J.C.; Hession, W.C. Vegetative impacts on hydraulics and sediment processes across the fluvial system. *J. Hydrol.* **2013**, *505*, 364–376. [CrossRef]
13. Christiansen, T.; Azlak, M.; Ivits-Wasser, E. Floodplains: A Natural System to Preserve and Restore. EEA Report. 2019. Available online: https://www.eea.europa.eu/publications/floodplains-a-natural-system-to-preserve-and-restore (accessed on 20 April 2022).
14. Verheij, S.; Fokkens, B.; Buijse, A.D. *A Pan-European Survey to Strengthen and Improve Policies and Strategic Planning Regarding River Continuity Restoration*; STOWA Report Number: 2021-20; European Centre for River Restoration (ECRR): Saulx-les-Chartreux, France, 2021.
15. Penna, N.; Coscarella, F.; D'Ippolito, A.; Gaudio, R. Effects of fluvial instability on the bed morphology in vegetated channels. *Environ. Fluid Mech.* **2022**, *22*, 619–644. [CrossRef]
16. Yen, B.C. Open channel flow resistance. *J. Hydraul. Eng.* **2002**, *128*, 20–39. [CrossRef]
17. Rowiński, P.M.; Västilä, K.; Aberle, J.; Järvelä, J.; Kalinowska, M. How vegetation can aid in coping with river management challenges: A brief review. *Ecohydrol. Hydrobiol.* **2018**, *18*, 345–354. [CrossRef]
18. Bonilla-Porras, J.A.; Armanini, A.; Crosato, A. Extended Einstein's parameters to include vegetation in existing bedload predictors. *Adv. Water Resour.* **2021**, *152*, 103928. [CrossRef]
19. Fathi-Moghadam, M.; Drikvandi, K.H. Manning roughness coefficient for rivers and flood plains with non-submerged vegetation. *Int. J. Hydraul. Eng.* **2012**, *1*, 1–4.
20. Eris, E.; Bombar, G.; Kavakli, Ü. Effect of emergent vegetation distribution on energy loss. In Proceedings of the 4th IAHR Europe Congress, Liege, Belgium, 27–29 July 2016.
21. Athikalam, P.T.; Vaideeswaran, A.K. Vegetation bioshield for coastal protection in South Asia: Status and way forward. *J. Coast. Conserv.* **2022**, *26*, 1–21. [CrossRef]
22. Bennett, S.J.; Simon, A. *Riparian Vegetation and Fluvial Geomorphology*; American Geophysical Union: Washington, DC, USA, 2004.
23. Green, J.C. Comparison of blockage factors in modelling the resistance of channels containing submerged macrophytes. *River Res. Appl.* **2005**, *21*, 671–686. [CrossRef]
24. Nepf, H.M. Hydrodynamics of vegetated channels. *J. Hydraul. Res.* **2012**, *50*, 262–279. [CrossRef]
25. Luhar, M.; Nepf, H.M. From the blade scale to the reach scale: A characterization of aquatic vegetative drag. *Adv. Water Resour.* **2013**, *51*, 305–316. [CrossRef]
26. Afzalimehr, H.; Dey, S. Influence of bank vegetation and gravel bed on velocity and Reynolds stress distributions. *Int. J. Sediment Res.* **2009**, *24*, 236–246. [CrossRef]
27. Rutherfurd, I.D.; Anderson, B.; Ladson, A. Managing the effects of riparian vegetation on flooding. In *Principles for Riparian Lands Management*; Lovett, S., Price, P., Eds.; Land and Water Australia: Canberra, Australia, 2007; p. 190.
28. Nabaei, S.F.; Afzalimehr, H.; Sui, J.; Kumar, B.; Nabaei, S.H. Investigation of the effect of vegetation on flow structures and turbulence anisotropy around semi-elliptical abutment. *Water* **2021**, *13*, 3108. [CrossRef]
29. Maji, S.; Hanmaiahgari, P.R.; Balachandar, R.; Pu, J.H.; Ricardo, A.M.; Ferreira, R.M. A Review on hydrodynamics of free surface flows in emergent vegetated channels. *Water* **2020**, *12*, 1218. [CrossRef]
30. Penna, N.; Coscarella, F.; D'Ippolito, A.; Gaudio, R. Bed roughness effects on the turbulence characteristics of flows through emergent rigid vegetation. *Water* **2020**, *12*, 2401. [CrossRef]
31. Penna, N.; Coscarella, F.; D'Ippolito, A.; Gaudio, R. Anisotropy in the free stream region of turbulent flows through emergent rigid vegetation on rough beds. *Water* **2020**, *12*, 2464. [CrossRef]
32. Caroppi, G.; Västilä, K.; Järvelä, J.; Rowiński, P.M.; Giugni, M. Turbulence at water-vegetation interface in open channel flow: Experiments with natural-like plants. *Adv. Water Resour.* **2019**, *127*, 180–191. [CrossRef]
33. Yang, Q.J.; Nepf, H.M. Impact of vegetation on bed load transport rate and bedform characteristics. *Water Resour. Res.* **2019**, *55*, 6109–6124. [CrossRef]
34. Armanini, A.; Cavedon, V. Bed-load through emergent vegetation. *Adv. Water Resour.* **2019**, *129*, 250–259. [CrossRef]
35. Zhao, T.; Nepf, H.M. Turbulence dictates bedload transport in vegetated channels without dependence on stem diameter and arrangement. *Geophys. Res. Lett.* **2021**, *48*, e2021GL095316. [CrossRef]

36. Vargas-Luna, A.; Crosato, A.; Calvani, G.; Uijttewaal, W.S.J. Representing plants as rigid cylinders in experiments and models. *Adv. Water Resour.* **2016**, *93*, 205–222. [CrossRef]
37. Sturm, T.W. *Open Channel Hydraulics*, 2nd ed.; McGraw-Hill: New York, NY, USA, 2010; p. 546.
38. Lauria, A.; Alfonsi, G. Numerical Investigation of Ski Jump Hydraulics. *J. Hydraul. Eng.* **2020**, *146*, 04020012. [CrossRef]
39. Lauria, A.; Alfonsi, G.; Tafarojnoruz, A.J.F. Flow pressure behavior downstream of ski jumps. *Fluids* **2020**, *5*, 168. [CrossRef]
40. Kim, S.J.; Stoesser, T. Closure modeling and direct simulation of vegetation drag in flow through emergent vegetation. *Water Resour. Res.* **2011**, *47*, 10511. [CrossRef]
41. Freeman, G.E.; Rahmeyer, W.J.; Copeland, R. *Determination of Resistance Due to Shrubs and Woody Vegetation*; ERDC/CHL TR-00-25; Engineer Research and Development Center, US Army Corps of Engineers: Vicksburg, MI, USA, 2000.
42. James, C.S.; Birkhead, A.L.; Jordanova, A.A.; Sullivan, J.J. Flow resistance of emergent vegetation. *J. Hydraul. Eng.* **2004**, *42*, 390–398. [CrossRef]
43. Armanini, A.; Righetti, M.; Grisenti, P. Direct measurement of vegetation resistance in prototype scale. *J. Hydraul. Res.* **2005**, *42*, 481–487. [CrossRef]
44. Caroppi, G.; Västilä, K.; Järvelä, J.; Lee, C.; Ji, U.; Kim, H.S.; Kim, S. Flow and wake characteristics associated with riparian vegetation patches: Results from field-scale experiments. *Hydrol. Processes.* **2022**, *36*, e14506. [CrossRef]
45. Aberle, J.; Järvelä, J. Flow resistance of emergent rigid and flexible floodplain vegetation. *J. Hydraul. Res.* **2013**, *51*, 33–45. [CrossRef]
46. Vargas-Luna, A.; Crosato, A.; Uijttewaal, W.S.J. Effects of vegetation on flow and sediment transport: Comparative analyses and validation of predicting models. *Earth Surf. Process. Landf.* **2015**, *40*, 157–176. [CrossRef]
47. Jalonen, J.; Järvelä, J. Estimation of drag forces caused by natural woody vegetation of different scales. *J. Hydrodyn.* **2014**, *26*, 608–623. [CrossRef]
48. Yerdelen, C.; Tayfur, G.; Ozyaman, C. The effect of leafless and tandem vegetation on streamflow resistance in open channels. In Proceedings of the 11th International Congress on Advances in Civil Engineering, Istanbul, Turkey, 21–25 October 2014.
49. Zhang, H.; Wang, Z.; Xu, W.; Wang, H. Determination of emergent vegetation effects on Manning's coefficient of gradually varied flow. *IEEE Access* **2019**, *7*, 146778–146790. [CrossRef]
50. Zhang, S.; Liu, M.; Li, G.; Zhang, J.; Chen, S. Impact of the contact area between vegetation stalks and water flow on the hydraulic characteristics of sloped land. *Arabian J. Geosci.* **2021**, *14*, 482. [CrossRef]
51. Schlichting, H. *Grenzschichttheorie (Boundary Layer Theory)*; Braun: Karlsruhe, Germany, 1982. (In German)
52. Cheng, N.S. Calculation of drag coefficient for array of emergent circular cylinder with pseudofluid model. *J. Hydraul. Eng.* **2013**, *139*, 602–611. [CrossRef]
53. Liu, X.; Zeng, Y. Drag coefficient for rigid vegetation in subcritical open-channel flow. *Environ. Fluid. Mech.* **2017**, *17*, 1035–1050. [CrossRef]
54. Sonnenwald, F.; Stovin, V.; Guymer, I. Estimating drag coefficient for arrays of rigid cylinders representing emergent vegetation. *J. Hydraul. Res.* **2018**, *57*, 591–597. [CrossRef]
55. D'Ippolito, A.; Calomino, F.; Alfonsi, G.; Lauria, A. Flow resistance in open channel due to vegetation at reach scale: A review. *Water* **2021**, *13*, 116. [CrossRef]
56. D'Ippolito, A.; Calomino, F.; Alfonsi, G.; Lauria, A. Drag coefficient of in-line emergent vegetation in open channel flow. *Int. J. River Basin Manag.* **2021**, *15*, 329–334. [CrossRef]
57. Liu, M.Y.; Huai, W.X.; Yang, Z.H.; Zeng, Y.H. A genetic programming-based model for drag coefficient of emergent vegetation in open channel flows. *Adv. Water Resour.* **2020**, *140*, 103582. [CrossRef]
58. Li, R.M.; Shen, H.W. Effect of tall vegetations on flow and sediment. *J. Hydraul. Div.* **1973**, *99*, 793–814. [CrossRef]
59. Petryk, S. Drag on Cylinders in Open Channel Flow. Ph.D. Thesis, Colorado State University, Fort Collins, CO, USA, 1969.
60. Tanino, Y.; Nepf, H.M. Laboratory investigation of mean drag in random array of rigid, emergent cylinders. *J. Hydraul. Eng.* **2008**, *134*, 34–41. [CrossRef]
61. Cheng, N.S.; Nguyen, H.T. Hydraulic radius for evaluating resistance induced by simulated emergent vegetation in open-channel flow. *J. Hydraul. Eng.* **2011**, *137*, 995–1004. [CrossRef]
62. Ishikawa, Y.; Mizuhara, K.; Ashida, S. Effect of density of trees on drag exerted on trees in river channels. *J. For. Res.* **2000**, *5*, 271–279. [CrossRef]
63. D'Ippolito, A.; Lauria, A.; Alfonsi, G.; Calomino, F. Investigation of flow resistance exerted by rigid emergent vegetation in open channel. *Acta Geophys.* **2019**, *67*, 971–986. [CrossRef]
64. Nepf, H.M. Drag, turbulence and diffusion in flow through emergent vegetation. *Water Resour. Res.* **1999**, *35*, 479–489. [CrossRef]
65. Lama, G.F.C.; Errico, A.; Francalanci, S.; Solari, L.; Preti, F.; Chirico, G.B. Evaluation of flow resistance models based on field experiments in a partly vegetated reclamation channel. *Geosciences* **2020**, *10*, 47. [CrossRef]
66. Yerdelen, C.; Ozyaman, C.; Mazdeh, A.M. Stem drag coefficient calculation using uniform and non-uniform assumption of flow. In Proceedings of the 3rd Space for Hydrology Workshop, ESA-ESRIN, Frascati, Italy, 15–17 September 2015.
67. Schoneboom, T.; Aberle, J.; Dittrich, A. Spatial variability, mean drag forces, and drag coefficients in an array of rigid cylinders. In *Experimental Methods in Hydraulic Research*; Rowinski, P., Ed.; Springer: Berlin/Heidelberg, Germany, 2011; Volume 1, pp. 255–265.